Two-Measurement Tomography of High-Dimensional Orbital Angular Momentum Entanglement

Yi Li (李逸),[1,*] Shuang-Yin Huang (黄双印),[1,2,3,*] Min Wang (王敏),[1] Chenghou Tu (涂成厚),[1] Xi-Lin Wang (汪喜林),[2,3] Yongnan Li (李勇男),[1,†] and Hui-Tian Wang (王慧田)[2,3,4,‡]

[1]*Key Laboratory of Weak-Light Nonlinear Photonics and School of Physics, Nankai University, Tianjin 300071, China*
[2]*National Laboratory of Solid State Microstructures and School of Physics, Nanjing University, Nanjing 210093, China*
[3]*Collaborative Innovation Center of Advanced Microstructures, Nanjing University, Nanjing 210093, China*
[4]*Collaborative Innovation Center of Extreme Optics, Shanxi University, Taiyuan 030006, China*

(Received 29 November 2021; accepted 9 January 2023; published 3 February 2023)

High-dimensional (HD) entanglement enables an encoding of more bits than in the two-dimensional case and promises to increase communication capacity over quantum channels and to improve robustness to noise. In practice, however, one of the central challenges is to devise efficient methods to quantify the HD entanglement explicitly. Full quantum state tomography is a standard technology to obtain all the information about the quantum state, but it becomes impractical because the required measurements increase exponentially with the dimension in HD systems. Hence, it is highly anticipated that a new method will be found for characterizing the HD entanglement with as few measurements as possible and without introducing unwarranted assumptions. Here, we present and demonstrate a scan-free tomography method independent of dimension, which only requires two measurements for the characterization of two-photon HD orbital angular momentum (OAM) entanglement. Taking Laguerre-Gaussian modes of photons as an example, the density matrices of OAM entangled states are experimentally reconstructed with very high fidelity. Our method is also generalized to the mixed HD OAM entanglement. Our results provide realistic approaches for quantifying more complex OAM entanglement in many scientific and engineering fields such as multiphoton HD quantum systems and quantum process tomography.

DOI: 10.1103/PhysRevLett.130.050805

Quantum entanglement is a key ingredient in a variety of quantum information processing, such as quantum teleportation [1–3], quantum superdense coding [4,5], quantum cryptography [6], and quantum imaging [7,8]. Encoding several qubits per transmitted photon yields significant benefits for increasing channel capacity and resistance to noise [9,10]. Hence, increasing the dimensionality of entangled quantum systems is one of the next key technological steps towards the realization of more practical quantum information protocols, and it also offers novel fundamental research possibilities in quantum physics [11,12]. Several discrete photonic degrees of freedom have been considered for the creation of entanglement in multiple dimensions, such as path [13,14], time [15,16], and frequency bins [17–19]. The entanglement is also embedded in the spatial mode [20–22], which occurs in an infinite dimensional Hilbert space and is receiving more attention as a powerful method in quantum information. However, for entanglement in any degree of freedom, the certification of experimentally generated high-dimensional (HD) entangled states is a crucial and difficult task [23].

To achieve this goal, some quantum tomographic methods are presented and demonstrated experimentally, such as traditional full quantum state tomography (FQST) [24–26], mutually unbiased bases tomography [27,28], and symmetric informationally complete positive-operator valued measure (POVM)-based quantum tomography [29,30]. Usually, these methods are based on the measurement of several POVMs in an ensemble of N identically prepared copies of the unknown states, and they require one to perform a large number of different measurements, making the traditional FQST impractical in high dimensions. One remaining challenge in quantum state tomography is the limited speed and efficiency of data acquisition for HD quantum states. To improve the characterization efficiency, two bases [31] and asymptotical locking tomography [32] were presented to obtain all the information about the bipartite d-dimensional entangled states using few measurements, less than $2d^2$ only. The machine learning method was demonstrated to compress HD data into low-dimensional representations and reduce the experimental burden of the FQST [33]. Compressive sensing technology was implemented for the tomography of HD pure states, which still increases the required measurements with the entanglement dimension [34,35]. In the direct tomography of HD quantum states reported recently, the data acquisition time is independent of the dimension, while the use of polarization-resolving cameras limits applications [36]. The interferometric method was reported to reduce the measurement complexity for characterizing

the density matrix, which theoretically requires $(d-1)$ measurements for reconstructing the pure states of d-dimensional qudits [37]. Direct measurement of the density matrix in the HD orbital angular momentum (OAM) basis was also reported, via scanning bucket detectors for data acquisition [38,39]. An approach for multiphoton states was also demonstrated by recovering structured quantum states from a single observable in a single experimental setup [40].

Here we present a scan-free tomography strategy for reconstructing the HD OAM entangled states using an intensified charge coupled device (ICCD) camera. In our scan-free tomography, only two measurements are required independent of dimension for two-photon entanglement. Taking the Laguerre-Gaussian (LG) mode as an example, we theoretically and experimentally show the characterization of two-photon OAM entangled states with high fidelity. Our strategy aims towards quantum information, and quantum communication can be generalized to other spatial modes carrying OAM, such as Bessel-Gaussian (BG) modes. Our certification method can also be used for mixed and multiphoton OAM entanglement, which is useful for the foundation of quantum mechanics.

The generated photon pairs are entangled in their OAM degree of freedom in $(2d+1)$ dimensions as

$$|\psi\rangle = \sum_{l=-d}^{d} \alpha_l \exp(j\phi_l)|l\rangle_s|-l\rangle_i, \tag{1}$$

where $|l\rangle_s$ or $|-l\rangle_i$ represents the single-photon OAM state with quantum number l (i.e., topological charge), for the signal (s) or idler (i) photons. Here, $\alpha_l \geq 0$ and $\phi_l \in [0, 2\pi)$ are the amplitude and phase for the state $|l\rangle_s|-l\rangle_i$. Additionally, α_l is the normalized coefficient, and α_l^2 is proportional to the probability $P_{l,-l}$ of detecting the signal photons in state $|l\rangle_s$ and the idler photons in state $|-l\rangle_i$. Here, $|l\rangle$ represents a zero-radial-index LG mode with a topological charge of l, which can construct a set of orthogonal and complete eigenmodes, where $|l\rangle \propto E_l(r)\exp(jl\varphi)$ in the cylindrical coordinates (r, φ, z) carries the OAM of $l\hbar$ per photon and $E_l(r)$ is the amplitude function at the beam waist (see Ref. [41] for details).

The traditional FQST for the OAM entanglement uses a spatial light modulator (SLM), together with a single-mode fiber (SMF), which acts as the mode filter to implement the projection measurements of the spatial states of photons by scanning the bucket detector. For a $(2d+1)$-dimensional entanglement, $2(2d+1)$ computer-generated holograms allow about $(2d+1)^4$ projection measurements on the selected bases to determine the density matrix [39]. The first task is to determine how to dramatically reduce the measurements. Unlike the traditional FQST, which needs to implement a large number of projection measurements using one-by-one single state scanning, our method requires only two projection measurements, using a pixel camera to capture the spatial intensity patterns rather than using a bucket detector to collect the total intensity only.

Here, we present the two-measurement tomography of HD OAM entanglement (see Ref. [41] for a general theory). As the principle schematic of our two-measurement tomography in Fig. 1(a), the entangled photon pairs (signal and idler photons) are generated by the spontaneous parametric down-conversion (SPDC) in a nonlinear crystal; the SLM can place the signal photons into two sets of OAM *superposition* states ($|\dot{\Psi}_s\rangle$ and $|\ddot{\Psi}_s\rangle$) instead of one-by-one single state scanning to implement two projection measurements. Then, the idler photons will be reduced to two sets of correlated OAM superposition states ($|\dot{\Psi}_i\rangle$ and $|\ddot{\Psi}_i\rangle$); the signal photons are coupled into a SMF and detected by an avalanche photon diode (APD), and the APD detector triggers a pixel intensified charge coupled

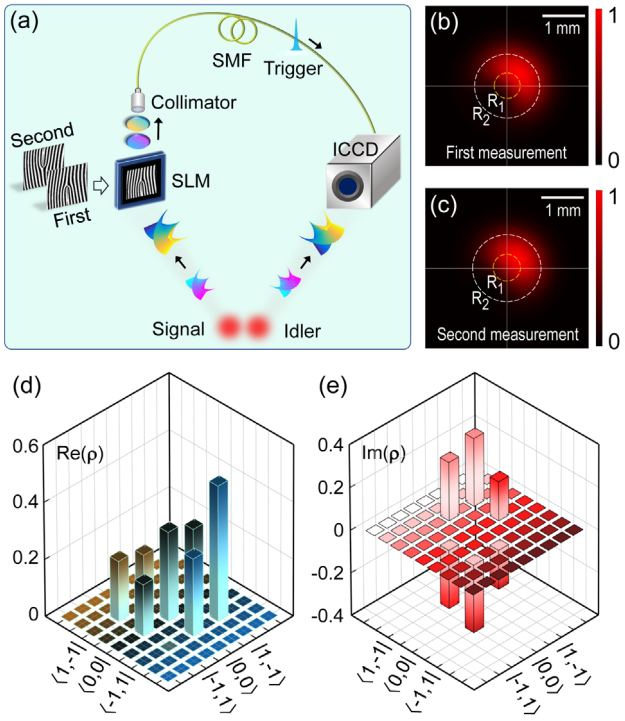

FIG. 1. Concept of two-measurement tomography and simulated tomographic reconstruction of a three-dimensional OAM entangled state. (a) Principle schematic of two-measurement tomography for measuring the OAM entangled states created by the SPDC process. Signal photons are measured in the superposition OAM basis with the SLM loaded in a suitable holography. The signal photons enter the single photon detector, and its electrical signal is used to trigger the ICCD camera. The spatial patterns of the reduced OAM superposition states of the idler photons are captured by the triggered ICCD camera. (b) [(c)] Simulated intensity pattern of the reduced OAM state of the idler photons under the projection basis $|\dot{\Psi}_s\rangle = (|0\rangle_s + |1\rangle_s)/\sqrt{2}$ $[|\ddot{\Psi}_s\rangle = (|0\rangle_s + |-1\rangle_s)/\sqrt{2}]$ of the signal photons. (d) [(e)] Simulated real [imaginary] part of the reconstructed density matrix for the preset three-dimensional OAM entangled target state shown in Eq. (2).

device (ICCD) camera to capture two images of the spatial coincidence distribution (i.e., the intensity distribution patterns of the idler photons) in the two projection measurements. It is of great importance that the two projection measurements have a shared single state such as $|0\rangle_s$, which builds a link between the two measurements.

To prove the validity of our method, we first carry out a simulation. We select a three-dimensional OAM entangled state $|\psi\rangle$ as the simulation target state (see Ref. [41] for details),

$$|\psi\rangle = [4\exp(j7\pi/4)|-1\rangle_s|1\rangle_i + 5|0\rangle_s|0\rangle_i + 6\exp(j\pi/4)|1\rangle_s|-1\rangle_i]/\sqrt{77}. \quad (2)$$

In our tomography, the coincidence patterns depend on the projection basis of the signal photons. Throughout this Letter, all the parameters related to the first and second measurements are defined by symbols with superjacent single dots and double dots, respectively. Under two projection bases, $|\dot{\Psi}_s\rangle = (|0\rangle_s + |1\rangle_s)/\sqrt{2}$ and $|\ddot{\Psi}_s\rangle = (|0\rangle_s + |-1\rangle_s)/\sqrt{2}$, we do not know the forms of the reduced states of the idler photons in practice, but we can experimentally capture the two coincidence images of the idler photons using the ICCD. If we measure the two coincidence images experimentally, both will be used to reconstruct the target entangled state and density matrix. We now give the simulation results of two spatial coincidence images of the idler photons (see Ref. [41] for details), as shown in Figs. 1(b) and 1(c). The important task is to obtain the amplitudes $\{\alpha_l\}$ and phases $\{\phi_l\}$ from the two simulated coincidence images in Figs. 1(b) and 1(c) to reconstruct the density matrix of the target state $|\psi\rangle$ in Eq. (2). Following our algorithm (see Ref. [41] for details), due to the interference between the reduced superposition states of the idler photons, the two images in Figs. 1(b) and 1(c), as a function of the radial coordinate R_p and the azimuthal coordinate φ, can be written as

$$\dot{I}(R_p,\varphi) = \dot{\kappa}[\alpha_0^2 E_0^2(R_p) + \alpha_1^2 E_{-1}^2(R_p) + 2\alpha_0\alpha_1 E_0(R_p)E_{-1}(R_p)\cos(\varphi-\phi_1)], \quad (3a)$$

$$\ddot{I}(R_p,\varphi) = \ddot{\kappa}[\alpha_0^2 E_0^2(R_p) + \alpha_{-1}^2 E_1^2(R_p) + 2\alpha_0\alpha_{-1} E_0(R_p)E_1(R_p)\cos(\varphi+\phi_{-1})], \quad (3b)$$

where $\dot{\kappa}$ and $\ddot{\kappa}$ are the proportional factors, which dominantly depend on by the detection efficiency of the detector. To solve the amplitudes $\{\alpha_l\}$ and phases $\{\phi_l\}$, we need to choose at least two circles with different radii (R_1 and R_2) as shown in Figs. 1(b) and 1(c). In fact, the intensity distribution along each circle in Figs. 1(b) and 1(c) can be expressed as the sum of a series of periodic (cosine) functions with different angular frequencies. For the three-dimensional entanglement, the angular frequencies should be 0 and 1; then they can be written as

$$\dot{I}(R_p) = \dot{b}_0^p + \dot{b}_1^p\cos(\varphi+\dot{\beta}_1^p), \quad (4a)$$

$$\ddot{I}(R_p) = \ddot{b}_0^p + \ddot{b}_1^p\cos(\varphi+\ddot{\beta}_1^p). \quad (4b)$$

The parameters, $\dot{b}_0^p, \dot{b}_1^p, \dot{\beta}_1^p, \ddot{b}_0^p, \ddot{b}_1^p$, and $\ddot{\beta}_1^p$ can be obtained by using a discrete Fourier transform (DFT). Comparing the parameters in Eqs. (3a) and (3b) with Eqs. (4a) and (4b), we can solve the amplitudes $\{\alpha_l\}$ and phases $\{\phi_l\}$. The simulation results give $\{\alpha_{-1}=0.460, \alpha_0=0.560, \alpha_1=0.690\}$ and $\{\phi_{-1}=5.500, \phi_0=0, \phi_1=0.795\}$ (see Ref. [41] for details), which are close to the preset values of $\{\alpha_{-1}=0.456, \alpha_0=0.570, \alpha_1=0.684\}$ and $\{\phi_{-1}=5.498, \phi_0=0, \phi_1=0.785\}$. If we choose more circles in Figs. 1(b) and 1(c), the reconstructed density matrix will have a more accurate fidelity using the mean method. When choosing 50 equal-interval concentric circles from either of the two images, the real and imaginary parts of the reconstructed density matrix of the target state $|\psi\rangle$ are shown in Figs. 1(d) and 1(e), the reconstructed state has a fidelity higher than 0.99. Therefore, our two-measurement tomography should be valid theoretically for characterizing the HD OAM entanglement.

We now implement experiments to test our tomography method (see Ref. [41] for details). We want to experimentally generate a two-qutrit OAM entangled target state $|\psi\rangle = 0.50|-1\rangle_s|1\rangle_i + 0.71|0\rangle_s|0\rangle_i + 0.50|1\rangle_s|-1\rangle_i$ by the SPDC in a type-II periodically poled potassium titanyl phosphate (PPKTP). We first characterize the quality of the generated state by the traditional FQST [24–26] and obtain the reconstructed state of $|\psi\rangle = 0.51|-1\rangle_s|1\rangle_i + 0.69|0\rangle_s|0\rangle_i + 0.51|1\rangle_s|-1\rangle_i$. The experimentally generated state has a fidelity beyond 0.99 with respect to the target state, implying that the quality of the OAM entangled state we generated is very high. We now experimentally explore our two-measurement tomography method. The output facet of the PPKTP crystal is imaged onto the ICCD plane. We use two superposition states, $|\dot{\Psi}_s\rangle = (|0\rangle_s + |1\rangle_s)/\sqrt{2}$ and $|\ddot{\Psi}_s\rangle = (|0\rangle_s + |-1\rangle_s)/\sqrt{2}$, as the projection bases of the signal photons. Two-measurement images (for the reduced idler photons) captured by the ICCD camera are shown in Figs. 2(a) and 2(b). Compared to the scanning of the bucket detector, direct imaging with the ICCD significantly shortens the time required for measurement. Hence, the real-time imaging with the ICCD has an improvement of many orders of magnitude both spatially and temporally, opening possible novel applications in quantum information and metrology. We set the intensifier gate width at 10 ns as the coincidence gate time to ensure that only the correlated idler photon events are registered. We adjust the exposure time to be 15 s to get enough of the detected idler photons for each of the two-measurement images. We extract the measured data on two

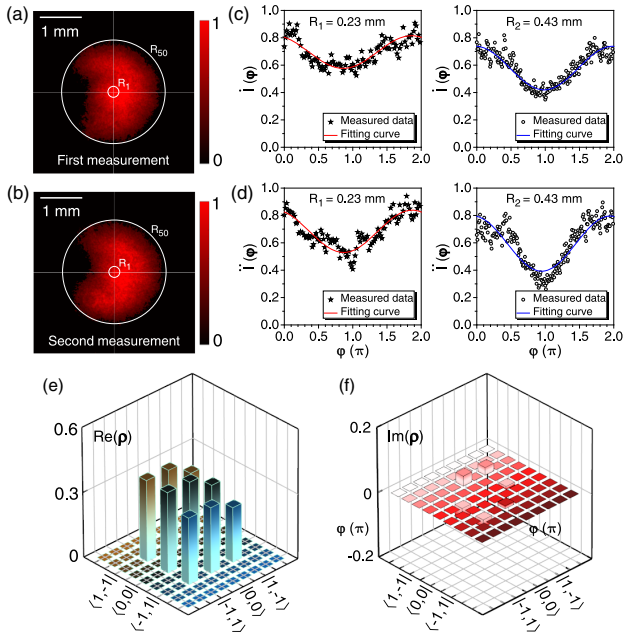

FIG. 2. Experimental results of a two-qutrit OAM entangled state. A two-qutrit OAM entangled state $|\psi\rangle = 0.50|-1\rangle_s|1\rangle_i + 0.71|0\rangle_s|0\rangle_i + 0.50|1\rangle_s|-1\rangle_i$ is the target state we want to experimentally generate by the SPDC process in a type-II ppKTP. (a) [(b)] Image measured by the ICCD in the first [second] measurement, under the projection basis $|\dot{\Psi}_s\rangle = (|0\rangle_s + |1\rangle_s)/\sqrt{2}$ $[|\ddot{\Psi}_s\rangle = (|0\rangle_s + |-1\rangle_s)/\sqrt{2}]$ for the signal photons. (c) [(d)] Measured data and fitting curves of two concentric circles (with radii of R_1 and R_2) from the image in (a) [(b)]. (e) [(f)] Real [imaginary] part of the reconstructed density index by choosing 50 equal-interval concentric circles (the radius has a range from 0.13 to 1.235 mm) from each of the two images.

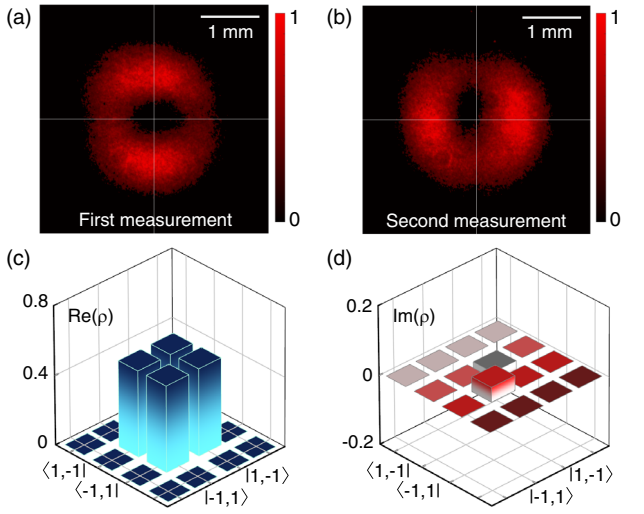

FIG. 3. Experimental results of a symmetric OAM entangled state. A symmetric OAM entangled state $|\psi\rangle = (|-1\rangle_s|1\rangle_i + |1\rangle_s|-1\rangle_i)/\sqrt{2}$ is experimentally generated as the target state by using the SPDC in a type-II ppKTP. (a) [(b)] Image measured by the ICCD in the first [second] measurement, under the projection basis $|\dot{\Psi}\rangle = (2|-1\rangle_s - |1\rangle_s)/\sqrt{5}$ $(|\ddot{\Psi}\rangle = (|-1\rangle_s + 2|1\rangle_s)/\sqrt{5})$ for the signal photons. (c) [(d)] Real [imaginary] part of the reconstructed density index by choosing 50 equal-interval concentric circles (the radius has a range from 0.26 to 1.30 mm) from each of two images in (a) and (b).

circles with radii of 0.23 mm and 0.43 mm from either of the two-measurement images in Figs. 2(a) and 2(b). By using the fitting red and blue curves in Figs. 2(c) and 2(d) of the data and our method (see Ref. [41] for details), we can reconstruct the target state. When choosing 50 equal-interval concentric circles from either of the two images, as shown in Figs. 2(e) and 2(f), the real and imaginary parts of the density matrix reconstructed with our two-measurement tomography show that the reconstructed state has a fidelity of $F = 0.970 \pm 0.003$ (see Ref. [41] for details). We also explore the dependence of the fidelity of the reconstructed density matrix on the number of circles selected (N) (see Ref. [41] for details).

We also experimentally prepare a symmetric OAM entangled state $|\psi\rangle = (|-1\rangle_s|1\rangle_i + |1\rangle_s|-1\rangle_i)/\sqrt{2}$ as another target state to confirm our method again. For such a symmetric state, we should choose the asymmetric states $|\dot{\Psi}_s\rangle = (2|-1\rangle_s - |1\rangle_s)/\sqrt{5}$ and $|\ddot{\Psi}_s\rangle = (|-1\rangle_s + 2|1\rangle_s)/\sqrt{5}$ as the projection bases of the signal photons. Under the two projection bases, we capture experimentally the two coincidence spatial images of the idler photons by the ICCD in Figs. 3(a) and 3(b). Based on our method [41], we also choose 50 equal-interval concentric circles from each of the two images in Figs. 3(a) and 3(b) to reconstruct the target state. We obtain the reconstructed state of $|\psi\rangle = 0.71\exp(-0.086j)|-1\rangle_s|1\rangle_i + 0.71|1\rangle_s|-1\rangle_i$ with a fidelity of $F = 0.990 \pm 0.002$ in Figs. 3(c) and 3(d).

In the above, we verified in both simulation and experiment that our two-measurement tomography is valid and practical for HD spatial mode entanglement. However, we realized experimentally the characterization of *three*-dimensional OAM entanglement, which is only limited by the nonuniform distribution of OAMs in the SPDC process because the photons with higher OAMs become very weak. Creating the uniform HD OAM entanglement source will still be a huge challenge in the future. Here, we also simulate the characterization of 11-dimensional OAM entanglement based on our method (see Ref. [41] for details). The 11-dimensional OAM entangled target state is preset. Under the projection bases of the signal photons, we simulate the coincidence images of the idler photons for two measurements. Although the simulated amplitude $\{\alpha_l\}$ and phases $\{\phi_l\}$ $(l = 0, \pm 1, \ldots, \pm 5)$ from six concentric circles only in each of the two images have some errors from the preset values (see Tables I and II in [41]), when we choose 50 equal-interval concentric circles in each of the two simulated coincidence images to obtain more values of the amplitudes and phases, then their mean values are used to reconstruct the density matrix with a fidelity of $F = 0.990 \pm 0.001$ (see Ref. [41] for details).

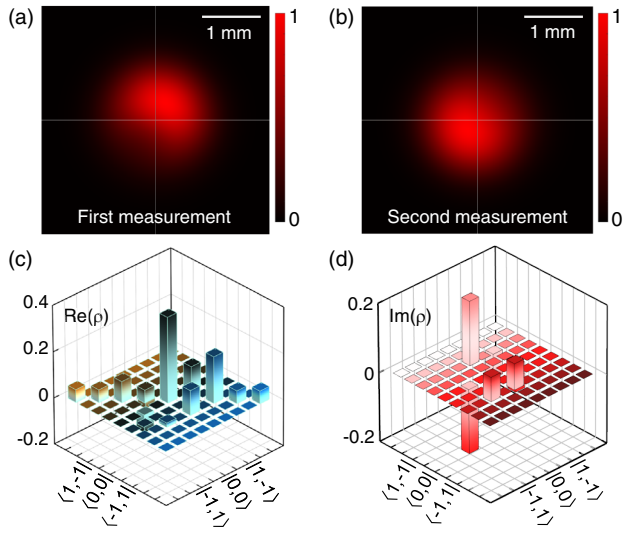

FIG. 4. Simulated reconstruction of three-dimensional OAM mixed entanglement state. The preset mixed target state is $\rho_w = I_9(1-x)/9 + x|\psi\rangle\langle\psi|$. Note that I_9 is a 9×9 identity matrix and $|\psi\rangle = [3|0\rangle_s|0\rangle_i + 2\exp(j\pi/3)|1\rangle_s|-1\rangle_i + \exp(j3\pi/4)|-1\rangle_s|1\rangle_i]/\sqrt{14}$. (a) [(b)] Simulated image that will be experimentally captured by the ICCD for the first [second] measurement, under the projection basis of $|\ddot{\Psi}_s\rangle = (|0\rangle + |1\rangle)/\sqrt{2}$ [$|\ddot{\Psi}_s\rangle = (|0\rangle + |-1\rangle)/\sqrt{2}$] for the signal photons. (c) [(d)] Real [imaginary] part of the reconstructed density matrix of ρ_w by choosing 50 equal-interval concentric circles from each of the two images. The radius has a range from 0.13 to 1.04 mm.

In general, only two measurements are needed for the characterization of the HD OAM entanglement due to the symmetric distribution of OAMs of photons in the SPDC process. In the recently demonstrated approaches [47–49], a superposition of OAM modes is imprinted by holograms into the pump beam, which translates via down-conversion into the asymmetric entangled states of two photons. For such kinds of states, one measurement is enough. In addition, the mixed entangled state has wide applications in both fundamental quantum mechanics and quantum information processing. Due to decoherence and dissipation, practical states are normally less entangled or partially mixed [50,51]. Obviously, quantifying the entanglement of mixed states is more complex than that of the pure ones, and it also becomes a challenge in many quantum technology applications. Our method is also valid for the mixed OAM entangled state (see Ref. [41] for details). As an example, we also used our two-measurement tomography to reconstruct the three-dimensional OAM mixed entangled state and the fidelity $F = 0.990 \pm 0.002$ (Fig. 4). Compared with the previous interferometric method, which is used to characterize the density matrix in the position basis, our method does not need additional interferometric schemes (Mach-Zehnder interferometry [36]), and it becomes more flexible and stable.

Conclusion.—We have proposed the practical method to characterize the HD OAM entanglement. Compared with the traditional FQST, our tomography method uses two-dimensional imaging detection instead of a scanning bucket detector. Besides its conceptual difference, our approach has another core strength: only two measurements are required to reconstruct the density matrix of the two-photon OAM entangled states. We confirmed the feasibility of our method by experimentally implementing the tomography of the two-photon three-dimensional OAM entangled states. Our idea can be extended to different families of spatial modes, such as BG modes carrying OAM [52,53] and Hermite-Gaussian modes without OAM. However, for any form of spatial mode entanglement, to detect the entanglement, the projection bases must be the corresponding eigenmodes and/or their superposition. Our method also has another very appealing feature: it is valid for mixed and multiphoton HD OAM entanglement (see Ref. [41] for details). We should emphasize that for an n-photon d-dimensional entangled state, our protocol needs $2(d^{n-1}-1)/(d-1)$ projection measurements at most, rather than two measurements, but the measurements are still much lower than other methods. Our scheme for direct tomography of the HD entanglement can be readily utilized not only in various applications such as superdense coding, HD quantum teleportation and quantum process tomography, but also for free-space communication [54] or even fiber-based [55] systems. The data acquisition time is independent of the entanglement dimension because our method needs two measurements for the two-photon entanglement, and the maximum dimension allowed by our protocol is only limited by the pixel count of the ICCD camera.

This work was supported financially by the National Key Research and Development Program of China (No. 2019YFA0705000, No. 2019YFA0308700, and No. 2020 YFA0309500) and the National Natural Science Foundation of China (No. 12234009, No. 12074196, No. 11922 406, and No. 12074197).

*These authors contributed equally to this work.
†Corresponding author.
liyongnan@nankai.edu.cn
‡Corresponding author.
htwang@nju.edu.cn

[1] J. G. Ren *et al.*, Ground-to-satellite quantum teleportation, Nature (London) **549**, 70 (2017).
[2] S. Pirandola, J. Eisert, C. Weedbrook, A. Furusawa, and S. L. Braunstein, Advances in quantum teleportation, Nat. Photonics **9**, 641 (2015).
[3] X. L. Wang, X. D. Cai, Z. E. Su, M. C. Chen, D. Wu, L. Li, N. L. Liu, C. Y. Lu, and J. W. Pan, Quantum teleportation of multiple degrees of freedom of a single photon, Nature (London) **518**, 516 (2015).

[4] L. J. Kong, R. Liu, W. R. Qi, Z. X. Wang, S. Y. Huang, Q. Wang, C. H. Tu, Y. N. Li, and H. T. Wang, Manipulation of eight-dimensional Bell-like states, Sci. Adv. **5**, eaat9206 (2019).
[5] X. M. Hu, Y. Guo, B. H. Liu, Y. F. Huang, C. F. Li, and G. C. Guo, Beating the channel capacity limit for superdense coding with entangled ququarts, Sci. Adv. **4**, eaat9304 (2018).
[6] J. Yin *et al.*, Entanglement-based secure quantum cryptography over 1,120 kilometres, Nature (London) **582**, 501 (2020).
[7] P. A. Moreau, E. Toninelli, T. Gregory, and M. J. Padgett, Imaging with quantum states of light, Nat. Rev. Phys. **1**, 367 (2019).
[8] H. Defienne, B. Ndagano, A. Lyons, and D. Faccio, Polarization entanglement-enabled quantum holography, Nat. Phys. **17**, 591 (2021).
[9] M. Erhard, M. Krenn, and A. Zeilinger, Advances in high-dimensional quantum entanglement, Nat. Rev. Phys. **2**, 365 (2020).
[10] M. Doda, M. Huber, G. Murta, M. Pivoluska, M. Plesch, and C. Vlachou, Quantum Key Distribution Overcoming Extreme Noise: Simultaneous Subspace Coding Using High-Dimensional Entanglement, Phys. Rev. Appl. **15**, 034003 (2021).
[11] L. Chen, W. Zhang, Z. Wu, J. Wang, R. Fickler, and E. Karimi, Experimental ladder proof of Hardy's nonlocality for high-dimensional quantum systems, Phys. Rev. A **96**, 022115 (2017).
[12] M. Hiekkamäki and R. Fickler, High-Dimensional Two-Photon Interference Effects in Spatial Modes, Phys. Rev. Lett. **126**, 123601 (2021).
[13] X. M. Hu, W. B. Xing, B. H. Liu, Y. F. Huang, C. F. Li, G. C. Guo, P. Erker, and M. Huber, Efficient Generation of High-Dimensional Entanglement through Multipath Down-Conversion, Phys. Rev. Lett. **125**, 090503 (2020).
[14] X. Qiang, X. Zhou, J. Wang, C. M. Wilkes, T. Loke, S. O'Gara, L. Kling, G. D. Marshall, R. Santagati, T. C. Ralph, J. B. Wang, J. L. O'Brien, M. G. Thompson, and J. C. F. Matthews, Large-scale silicon quantum photonics implementing arbitrary two-qubit processing, Nat. Photonics **12**, 534 (2018).
[15] A. Martin, T. Guerreiro, A. Tiranov, S. Designolle, F. Fröwis, N. Brunner, M. Huber, and N. Gisin, Quantifying Photonic High-Dimensional Entanglement, Phys. Rev. Lett. **118**, 110501 (2017).
[16] T. Zhong, H. Zhou, R. D. Horansky, C. Lee, V. B. Verma, A. E. Lita, A. Restelli, J. C. Bienfang, R. P. Mirin, T. Gerrits, S. W. Nam, F. Marsili, M. D. Shaw, Z. Zhang, L. Wang, D. Englund, G. W. Wornell, J. H. Shapiro, and F. N. C. Wong, Photon-efficient quantum key distribution using time-energy entanglement with high-dimensional encoding, New J. Phys. **17**, 022002 (2015).
[17] M. Kues, C. Reimer, J. M. Lukens, W. J. Munro, A. M. Weiner, D. J. Moss, and R. Morandotti, Quantum optical microcombs, Nat. Photonics **13**, 170 (2019).
[18] C. Reimer, M. Kues, P. Roztocki, B. Wetzel, F. Grazioso, B. E. Little, S. T. Chu, T. Johnston, Y. Bromberg, L. Caspani, D. J. Moss, and R. Morandotti, Generation of multiphoton entangled quantum states by means of integrated frequency combs, Science **351**, 1176 (2016).
[19] M. Kues, C. Reimer, P. Roztocki, L. R. Cortés, S. Sciara, B. Wetzel, Y. Zhang, A. Cino, S. T. Chu, B. E. Little, D. J. Moss, L. Caspani, J. Azaña, and R. Morandotti, On-chip generation of high-dimensional entangled quantum states and their coherent control, Nature (London) **546**, 622 (2017).
[20] H. Cao, S. C. Gao, C. Zhang, J. Wang, D. Y. He, B. H. Liu, Z. W. Zhou, Y. J. Chen, Z. H. Li, S. Y. Yu, J. Romero, Y. F. Huang, C. F. Li, and G. C. Guo, Distribution of high-dimensional orbital angular momentum entanglement over a 1 km few-mode fiber, Optica **7**, 232 (2020).
[21] M. Krenn, M. Huber, R. Fickler, R. Lapkiewicz, S. Ramelow, and A. Zeilinger, Generation and confirmation of a (100×100)-dimensional entangled quantum system, Proc. Natl. Acad. Sci. U.S.A. **111**, 6243 (2014).
[22] M. Erhard, R. Fickler, M. Krenn, and A. Zeilinger, Twisted photons: New quantum perspectives in high dimensions, Light **7**, 17146 (2018).
[23] N. Friis, G. Vitagliano, M. Malik, and M. Huber, Entanglement certification from theory to experiment, Nat. Rev. Phys. **1**, 72 (2019).
[24] B. Jack, J. Leach, H. Ritsch, S. M. Barnett, M. J. Padgett, and S. Franke-Arnold, Precise quantum tomography of photon pairs with entangled orbital angular momentum, New J. Phys. **11**, 103024 (2009).
[25] M. Agnew, J. Leach, M. McLaren, F. S. Roux, and R. W. Boyd, Tomography of the quantum state of photons entangled in high dimensions, Phys. Rev. A **84**, 062101 (2011).
[26] E. Toninelli, B. Ndagano, A. Vallés, B. Sephton, I. Nape, A. Ambrosio, F. Capasso, M. J. Padgett, and A. Forbes, Concepts in quantum state tomography and classical implementation with intense light: A tutorial, Adv. Opt. Photonics **11**, 67 (2019).
[27] D. Giovannini, J. Romero, J. Leach, A. Dudley, A. Forbes, and M. J. Padgett, Characterization of High-Dimensional Entangled Systems via Mutually Unbiased Measurements, Phys. Rev. Lett. **110**, 143601 (2013).
[28] P. Erker, M. Krenn, and M. Huber, Quantifying high dimensional entanglement with two mutually unbiased bases, Quantum **1**, 22 (2017).
[29] W. M. Pimenta, B. Marques, T. O. Maciel, R. O. Vianna, A. Delgado, C. Saavedra, and S. Pádua, Minimum tomography of two entangled qutrits using local measurements of one-qutrit symmetric informationally complete positive operator-valued measure, Phys. Rev. A **88**, 012112 (2013).
[30] N. Bent, H. Qassim, A. A. Tahir, D. Sych, G. Leuchs, L. L. Sánchez-Soto, E. Karimi, and R. W. Boyd, Experimental Realization of Quantum Tomography of Photonic Qudits via Symmetric Informationally Complete Positive Operator-Valued Measures, Phys. Rev. X **5**, 041006 (2015).
[31] J. Bavaresco, N. H. Valencia, C. Klöckl, M. Pivoluska, P. Erker, N. Friis, M. Malik, and M. Huber, Measurements in two bases are sufficient for certifying high-dimensional entanglement, Nat. Phys. **14**, 1032 (2018).
[32] L. J. Kong, R. Liu, W. R. Qi, Z. X. Wang, S. Y. Huang, C. H. Tu, Y. N. Li, and H. T. Wang, Asymptotical locking

tomography of high-dimensional entanglement, Chin. Phys. Lett. **37**, 034204 (2020).
[33] G. Torlai, G. Mazzola, J. Carrasquilla, M. Troyer, R. Melko, and G. Carleo, Neural-network quantum state tomography, Nat. Phys. **14**, 447 (2018).
[34] M. Mirhosseini, O. S. Magaña-Loaiza, S. M. H. Rafsanjani, and R. W. Boyd, Compressive Direct Measurement of the Quantum Wave Function, Phys. Rev. Lett. **113**, 090402 (2014).
[35] D. Gross, Y. K. Liu, S. T. Flammia, S. Becker, and J. Eisert, Quantum State Tomography via Compressed Sensing, Phys. Rev. Lett. **105**, 150401 (2010).
[36] Y. Zhou, J. Zhao, D. Hay, K. McGonagle, R. W. Boyd, and Z. Shi, Direct Tomography of High-Dimensional Density Matrices for General Quantum States of Photons, Phys. Rev. Lett. **127**, 040402 (2021).
[37] S. N. Sahoo, S. Chakraborti, A. K. Pati, and U. Sinha, Quantum State Interferography, Phys. Rev. Lett. **125**, 123601 (2020).
[38] M. Malik, M. Mirhosseini, M. P. J. Lavery, J. Leach, M. J. Padgett, and R. W. Boyd, Direct measurement of a 27-dimensional orbital-angular-momentum state vector, Nat. Commun. **5**, 3115 (2014).
[39] M. Mirhosseini, O. S. Magaña-Loaiza, C. Chen, S. M. H. Rafsanjani, and R. W. Boyd, Wigner Distribution of Twisted Photons, Phys. Rev. Lett. **116**, 130402 (2016).
[40] D. Oren, M. Mutzafi, Y. C. Eldar, and M. Segev, Quantum state tomography with a single measurement setup, Optica **4**, 993 (2017).
[41] See Supplemental Material at http://link.aps.org/supplemental/10.1103/PhysRevLett.130.050805 for detailed theory and experiments, which includes Refs. [22,42–46].
[42] R. Fickler, M. Krenn, R. Lapkiewicz, S. Ramelow, and A. Zeilinger, Real-time imaging of quantum entanglement, Sci. Rep. **3**, 1914 (2013).
[43] N. A. Peters, J. B. Altepeter, D. Branning, E. R. Jeffrey, T. C. Wei, and P. G. Kwiat, Maximally entangled mixed states: Creation and concentration, Phys. Rev. Lett. **92**, 133601 (2004).
[44] Y. S. Zhang, Y. F. Huang, C. F. Li, and G. C. Guo, Experimental preparation of the Werner state via spontaneous parametric down-conversion, Phys. Rev. A **66**, 062315 (2002).
[45] M. Shutova, A. A. Zhdanova, and A. V. Sokolov, Detection of mixed OAM states via vortex breakup, Phys. Lett. A **381**, 408 (2017).
[46] M. Malik, M. Erhard, M. Huber, M. Krenn, R. Fickler, and A. Zeilinger, Multi-photon entanglement in high dimensions, Nat. Photonics **10**, 248 (2016).
[47] J. Kysela, M. Erhard, A. Hochrainer, M. Krenn, and A. Zeilinger, Path identity as a source of high-dimensional entanglement, Proc. Natl. Acad. Sci. U.S.A. **117**, 26118 (2020).
[48] Y. Chen, W. Zhang, D. Zhang, X. Qiu, and L. Chen, Coherent Generation of the Complete High-Dimensional Bell Basis by Adaptive Pump Modulation, Phys. Rev. Appl. **14**, 054069 (2020).
[49] E. V. Kovlakov, S. S. Straupe, and S. P. Kulik, Quantum state engineering with twisted photons via adaptive shaping of the pump beam, Phys. Rev. A **98**, 060301(R) (2018).
[50] J. W. Pan, S. Gasparoni, R. Ursin, G. Weihs, and A. Zeilinger, Experimental entanglement purification of arbitrary unknown states, Nature (London) **423**, 417 (2003).
[51] A. Vaziri, J. W. Pan, T. Jennewein, G. Weihs, and A. Zeilinger, Concentration of Higher Dimensional Entanglement: Qutrits of Photon Orbital Angular Momentum, Phys. Rev. Lett. **91**, 227902 (2003).
[52] M. McLaren, M. Agnew, J. Leach, F. S. Roux, M. J. Padgett, R. W. Boyd, and A. Forbes, Entangled Bessel-Gaussian beams, Opt. Express **20**, 23589 (2012).
[53] M. McLaren, T. Mhlanga, M. J. Padgett, F. S. Roux, and A. Forbes, Self-healing of quantum entanglement after an obstruction, Nat. Commun. **5**, 3248 (2014).
[54] V. D'Ambrosio, E. Nagali, S. P. Walborn, L. Aolita, S. Slussarenko, L. Marrucci, and F. Sciarrino, Complete experimental toolbox for alignment-free quantum communication, Nat. Commun. **3**, 961 (2012).
[55] J. Liu, I. Nape, Q. Wang, A. Vallés, J. Wang, and A. Forbes, Multidimensional entanglement transport through single-mode fiber, Sci. Adv. **6**, eaay0837 (2020).